

Impact and Embedding of Picoliter Droplets into Freely Suspended Smectic Films

Sarah Dölle,* Kirsten Harth, Thomas John,[†] and Ralf Stannarius*

Department of Nonlinear Phenomena, Otto von Guericke University Magdeburg, PB 4120, 39016 Magdeburg, Germany

Supporting Information

ABSTRACT: We study the impact of liquid microdroplets on thin freely suspended smectic films. Such films are very thin but robust objects that can serve as model systems for quasi-two-dimensional liquids. Droplet velocities and sizes determine the character of the collisions. The dynamics of the integration of droplets into the film can be divided into three phases, starting with the impact and a dissipation of the kinetic energy, followed by a balancing of capillary forces within fractions of a second. The analysis of the droplet shape evolution with high-speed imaging allows us to study the dynamics of this process. The final phase, formation of a meniscus of smectic material, takes several seconds up to minutes.



INTRODUCTION

Droplet impacts on liquid surfaces generate interesting phenomena, related for example to wetting and splashing. The process of droplet impact has been studied for over a century, starting with Worthington's pioneering work *The Splash of a Drop* in 1895.¹ Most of the experimental and theoretical work dealt basically with impacts on compact matter such as deep liquid pools,^{2,3,6–10} other droplets,^{11,12} thin liquid layers on solid substrates,^{13–16} or solid substrates.^{17–27} A summary of different types of dynamic behavior of impacting droplets can be found, for example, in the review article by Yarin.²⁸

High-speed imaging²⁹ has triggered substantial progress in this field during recent years. By now, such phenomena as splashing, rebound, and deposition of droplets on smooth solid surfaces have been extensively studied and they are fairly well understood. Recent experiments focused, for example, on the role of air pressure during splashing.^{18–25} The vast majority of experiments dealt with macroscopic drops.^{13,30–33} This knowledge cannot be transferred straightforwardly to the dynamics of micrometer-sized droplets: Inertial, capillary, and viscous forces have to be taken in consideration during droplet impact. In principle, four different impact scenarios can be distinguished by characteristic Weber (*We*) and Ohnesorge (*Oh*) numbers:³⁴

$$We = \frac{l\rho v^2}{\sigma} \quad Oh = \frac{\eta}{\sqrt{\rho\sigma l}} = \frac{We}{\sqrt{Re}} \quad (1)$$

The Weber number can be described as a ratio between kinetic and capillary energies, where σ is the surface tension, l is the diameter of the droplet, ρ is its density, and v is the velocity. The Ohnesorge number relates the viscous force (dynamic viscosity η) to inertial and capillary forces. In regime I with $We \gg 1$ and $Oh \ll (We)^{1/2}$, the dominant driving force is the impact pressure primarily restrained by inertia. The fluid can be considered as almost inviscid, and it shows a rapid spreading followed by underdamped interfacial oscillations. In regime II with $We \ll 1$ and $Oh \ll 1$, the fluid still appears inviscid, but impact velocity generated effects are negligible. The imbalance of the capillary

force at the contact line should drive the initial spreading. In regimes III and IV, viscosity effects become more important than inertia effects, leading to an overdamped motion without oscillations. In regime III with $We \ll 1$ and $Oh \gg 1$, spreading is driven by the capillary force. In regime IV, the behavior is dependent on the impact velocity, with $We \gg 1$ and $Oh \gg (We)^{1/2}$.

Many researchers studied the spreading effects of droplets with Reynolds numbers between 100 and 2000 and Weber numbers between 1 and 400 for droplets of 200–3000 μm diameter.^{13,21,31,32,35,36} Impacts of droplets with diameters in the micrometer range have been investigated, for example, in refs 37 and 38.

With the development of microdispensing, a strong interest in the impact scenarios of micrometer-sized droplets on different substrates evolved. Droplet dispensing technologies contributed to diverse fields like semiconductor packaging, bioprinting, and inkjet printing. The possibility of placing small volumes like single cells or DNA strands is particularly interesting for biological applications. Understanding the dynamics of small, sub-millimeter-sized droplets is a crucial step in upgrading existing technology and developing new applications. In this respect, interactions with soft substrates such as liquid crystalline membranes are particularly interesting. Several studies were devoted to the impact of droplets on soap or surfactant films,^{39–42} including the description of bouncing³⁹ and tunneling^{44–42} phenomena. In these experiments, film materials were aqueous soap solutions or oily inks. Even though these studies revealed interesting dynamical regimes, their interpretation is not straightforward because the film thickness in such materials is usually not uniform, and often not constant over time because of drainage. Insufficient magnification and time resolution prevented description of the actual impact process in detail.

Received: August 5, 2014

Revised: September 26, 2014

Published: September 30, 2014

Smectic films offer an alternative with several advantages over soap films. They are robust and not subject to drainage. Smectic freely suspended films (FSFs) can be prepared with well-defined and uniform thicknesses from two molecular layers to several hundred layers. They can serve as models to study structure and dynamics in reduced dimensionality.^{43,44} With suitable choice of impact parameters, one can achieve the incorporation of immiscible droplets in the films as objects for hydrodynamic studies in quasi-2D geometry. Films in different smectic phases can either resemble in-plane isotropic (smectic A) or anisotropic (smectic C) fluids. In the latter, anisotropy adds interesting effects: for example, the cross-coupling of local director orientation and the motion of inclusions.

Such films have been extensively studied in the past. In particular, shapes and interactions of solid and liquid inclusions in FSFs have been the focus of several studies.^{45–53} In most of these experiments, the liquid inclusions consist of the same fluid as the film. The samples are heated to the phase transition temperature, which leads to the formation of droplets consisting of isotropic melt. Naturally, this procedure cannot be used to prepare controlled droplet shapes or individual droplets. The temperature must be controlled precisely when one is interested in the study of stationary droplets, and the temperature range is strongly restricted. The procedure described in the present paper provides a suitable alternative: picoliter droplets of an immiscible fluid are shot onto a film in the smectic A phase. A piezoelectric dispenser can be controlled to produce droplets with variable speeds and firing rates. Inclusions of different sizes in the film can be prepared by shooting multiple droplets onto the same film spot, where they merge to form larger inclusions.

The interactions of picoliter droplets with the films are complex, and for a given droplet size they are mainly determined by the impact parameters. Bouncing, immersion and tunneling scenarios are observed depending on impact speed. Sufficiently slow droplets are caught by the films and gradually embedded. Droplets impacting in some intermediate speed range (velocities on the order of 4 m/s) bounce back from the deflected films after impact. At still higher speeds, the droplets penetrate the film plane and leave the film on the opposite side, whereby they become wrapped in a coating by the film material and leave an intact film after penetration. Such tunneling and encasement of a drop, in soap films, was already described in 2005 by Thoroddsen et al.⁴ Bouncing and tunneling are not considered in this study. Instead, we focus only on the incorporation of droplet material in the films, which can be divided into three distinct phases mainly governed by the balances of capillary forces. High-speed microscopic imaging allows us to study the process from impact

to immersion and relaxation to an equilibrium droplet shape. In a subsequent period of several seconds, the equilibrium shape of a meniscus is established; this phase can be observed with conventional video techniques.

EXPERIMENTAL SECTION

Materials. All experiments are performed with a five-compound mixture:

4-(hexyloxy)phenyl 4'-methoxybenzoate	17.6%
4-(octyloxy)phenyl 4'-(pentyloxy)benzoate	24.3%
4-(heptyloxy)phenyl 4'-hexylbenzoate	10.6%
4-(butyloxy)phenyl 4'-hexylbenzoate	27.5%
4-nitrophenyl 4'-(octyloxy)benzoate	20%

(obtained from W. Weissflog, Halle University). A mixture of the first four compounds is known as Mischung 5; it exhibits a nematic phase over a broad temperature range.^{54,55} Addition of a certain amount of 4-nitrophenyl 4'-(octyloxy)benzoate to Mischung 5 induces a smectic A (SmA) phase that is stable in a wide range above and below room temperature. The droplet material is an aqueous solution with 5% ethylene glycol. Ethylene glycol was purchased from Merck with a purity of at least 99%. The addition of ethylene glycol to water prohibits complete evaporation of the droplet during the experimental time scale (seconds to minutes for the long-term experiments). The droplet material is not miscible with the liquid crystal. An aqueous solution containing 0.1 mg/mL rhodamine 6G and 5% ethylene glycol is used for the fluorescence measurements.

Methods. Freely suspended films are drawn manually on the opening of a glass capillary (Figure 1) with inner diameter of about 4 mm, by use of a razor blade. The film thickness is estimated from the optical transmission of the film and the reflective interference colors. It is in the range of few hundred nanometers, not exceeding 500 nm. The FSF is bulged outward by subtle overpressure (\approx 50 Pa) in the capillary, which deforms it to approximately a hemisphere. This allows us to observe the side view of impacting droplets. The radius of curvature of the film is roughly 2 mm; the mean curvature is therefore negligible for the experiment.

Droplets are shot onto the film by means of a microdispenser, jetting device MJ-ATP-01, from MicroFab Technologies. The dispenser nozzle is a piezo-ceramic actuator with a diameter of about 43 μ m. After ejection, the droplets have spherical shape with a diameter of 40 μ m. This corresponds to droplet volumes of about 34 pL and masses of about 34 ng. The droplet velocity is adjusted by the driving voltage applied to the dispenser. We determine the impact velocities directly from the high-speed videos.

The observations are made by use of a long-range microscope (Questar QM 100, see Figure 1). Illumination is achieved by a 3 A light-emitting diode (Cree XM-L T6 emitter, LED-TECH), focused with a collimator lens. A high-speed camera (Phantom V611, Vision Research) is employed at a frame rate of 180 067 frames per second with an exposure time of 5.1 μ s. This allows us to record image sizes of

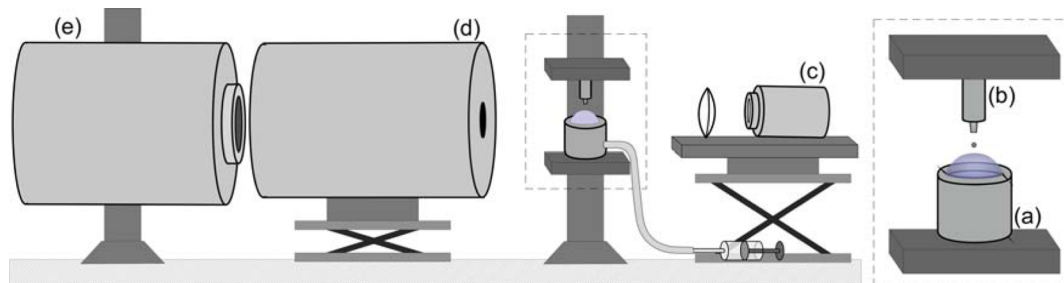


Figure 1. Schematic sketch of experimental setup. The opening of a glass capillary (a) is covered with a FSF. The film is bulged by slight overpressure, adjusted manually with a syringe connected to the capillary. A microdispenser (b) creates droplets with well-defined size and speed. The droplets are ejected vertically toward the center of the horizontal top of the FSF. An LED lamp (c) combined with a focusing lens is used for illumination. The impact process is recorded by a high-speed camera (e) attached to a long-range microscope (d).

128 pixel \times 128 pixel with $0.86 \mu\text{m}/\text{Pix}$ resolution. The necessary high illumination intensities set the limits to achieve suitable frame rates at the required magnifications and spatial resolutions.

RESULTS AND DISCUSSION

The dynamics of a droplet that is shot onto a freely suspended smectic film can be roughly divided into three phases, with very different time scales: in the first phase, the kinetic energy of the droplet is transformed into surface energy of the film and the droplet due to deformations, kinetic energy of the film and other forms, and a substantial part of the energy is dissipated. This process occurs on the scale of a few microseconds. In the second phase, the droplet changes shape and position in the film to reach a certain balance of capillary forces. This phase takes approximately 1 ms. The third phase is the formation of a meniscus of smectic material, which can take up to several seconds. All three phases are described in detail in the following sections.

Droplet Impact. In our study, picoliter droplets with diameters of about $40 \mu\text{m}$ and impact velocities between 0.4 and 2.5 m/s give Weber numbers between 0.1 and 3.8. The Ohnesorge number Oh is approximately 0.037; that is, viscosity effects are small in comparison to the influences of the surface tension. Thus, our experiment can be classified between regimes I and II introduced above. The droplet fluid can be treated as inviscid, as surface tensions play the essential role.

Figure 2 shows the impact of two aqueous ethylene glycol (5 wt %) droplets on a FSF. The droplet in the upper section of Figure 2 impacts with a velocity of 0.8 m/s , while the second droplet impacts with 2.5 m/s (Figure 2, bottom). The smectic film is hardly seen in the video images. From the detailed droplet shapes, it is possible to estimate the vertical level of the contact line of the film, which is marked by a horizontal bar in each image.

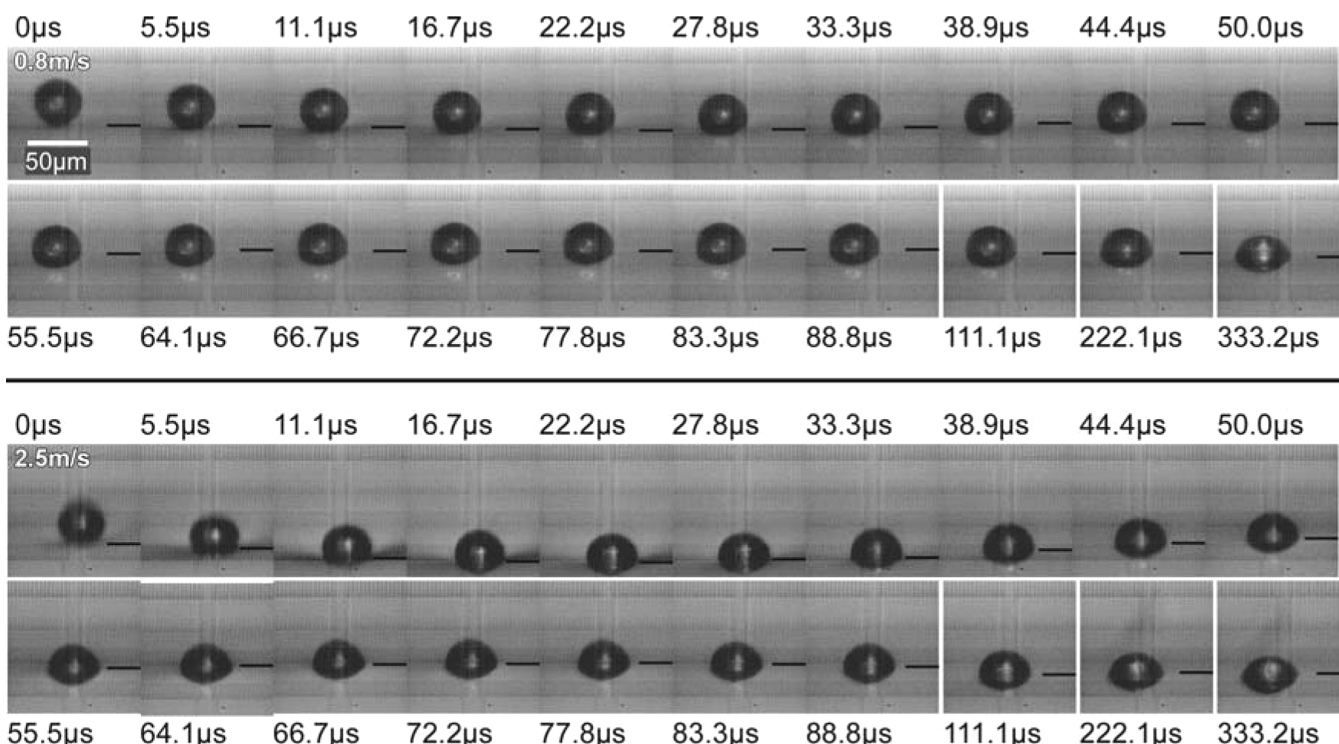


Figure 2. Photo sequence of droplet impact on a smectic FSF (side view). The upper two rows show a droplet impacting with a velocity of 0.8 m/s . The lower two rows show the impact of a droplet with an impact velocity of 2.5 m/s . The pictures were taken at a rate of 180 067 frames per second, by use of the setup shown in Figure 1. Black lines indicate the level of the line of contact with the film.

The film is displaced upon impact and it performs damped oscillations back to its original shape, with frequencies of roughly 10 kHz . With an initial kinetic energy of the fast droplet (Figure 2, bottom) of 0.11 nJ and an initial deflection of the film of about $30 \mu\text{m}$, one can estimate a force of about $3.6 \mu\text{N}$ decelerating the droplet. Most of the kinetic energy is transformed into a displacement and deflection of the film. In images obtained with a larger field of view, one can observe that the impact creates a catenoid-like local membrane deformation with a radius of roughly $200\text{--}300 \mu\text{m}$. This diameter is consistent with the observed film vibration frequency. [For oscillation spectra of smectic FSF, see ref 56. Compared to the dynamics of the bare film, one has to take into account here that the droplet mass is comparable to the effective film mass, slowing down the oscillation frequency by a factor of roughly $^{1/2}$].

A simplified back-of-the-envelope calculation can be used to estimate the work related to membrane displacement. The film is pushed against the overpressure in the capillary. If the area of the displaced part of the membrane is about $20 \times 10^{-8} \text{ m}^2$, and a mean displacement of $10 \mu\text{m}$ is assumed, then the work needed to compress the air is on the order of 50 pJ . A comparable part of the kinetic energy is stored as surplus surface energy of the deflected film, and some fraction is dissipated. For the slow droplet (0.8 m/s), the kinetic energy is 1 order of magnitude smaller and the film deflection is hardly resolved in the images.

The dynamics of droplet oscillations that might arise after impact may be estimated with Lamb's model⁵⁷ and the equation

$$\omega_m = \sqrt{\frac{m(m+1)(m-1)(m+2)\sigma}{[(m+1)\rho_i + m\rho_0]R^3}} \quad (2)$$

where ω_m is the angular frequency of the m th mode, ρ_i is the density of the droplet, ρ_0 is the density of air, and σ is the surface

tension of the liquid. The radius R of the droplet and the mode number m are the two major parameters. Lamb's model assumes inviscid fluids and vortex free flow. It can be widely used in hydrodynamics, for example, to describe the behavior of rain drops or fluid structures in biological cells. The fundamental oscillation mode has $m = 2$. For our micrometer-sized droplets, $\omega_2/2\pi$ is predicted to be around 1 MHz. With our time resolution limited to 5.5 μ s/frame, such oscillations cannot be detected. Apparently, they have low amplitudes and decay rapidly. The droplet hits the film almost like a solid object. A triple contact line⁵ between droplet, air, and film is formed. Already a few microseconds after impact, the droplet adopts a characteristic shape, and the upper part of the droplet above the initial contact line turns into a spherical cap (Figure 3).

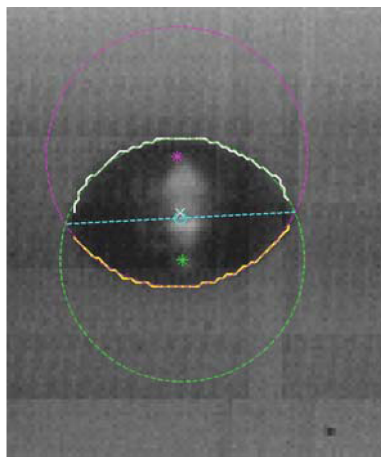


Figure 3. Typical droplet shape, 383 μ s after first contact. The two bright (white and yellow) curves mark the automatically detected droplet profiles, while the dark (green and magenta) circles are best fits. The straight line connects the two contact points and marks the contact line of the film at the droplet surface. Crosses mark the centers of the two virtual spheres that form the caps.

Embedding of the Droplet in the Film. Initially, the droplet is placed entirely on top of the film (here and in the following, we choose the references for top and bottom with respect to a droplet moving downward before impact), as is seen in the first two or three images of Figure 2. Then we observe the second phase, the gradual incorporation of the droplet into the smectic film. During this phase, the droplet can be fitted very well by two spherical caps that are linked to each other at the contact

line of the film. An example of such a fit is given in Figure 3. The image shows a droplet several hundred milliseconds after impact, when it is completely embedded in the film. Droplet profiles (bright lines) are detected automatically and circular arcs are fitted to the profiles.

In the first 100 ms, when the droplet rests upon the film, only the radius of curvature R_t of the top surface can be determined with sufficient accuracy. When the drop gradually sinks into the film plane, one can extract both radii of curvature. Figure 4 shows the typical evolution of the ratio of radii of curvature R_t and R_b (top and bottom) for a droplet at 0.4 m/s. Triangles mark values determined manually, and they have a larger uncertainty. Initially, the two radii differ by more than 30%. Within about 1 ms after impact, they equilibrate.

At a given pressure inside the droplet, the mean curvatures in equilibrium must be proportional to the respective interfacial tensions of both caps. We can neglect the small overpressure that adds to the atmospheric pressure below the bulged smectic film. (Actually, the Laplace pressure difference at the bottom surface of the droplet is slightly lower than at its top surface, but this gives only a small correction of about 1% to the radius ratio.)

The contact line of the free-standing film sets boundary conditions for the two caps. The differing initial curvatures can be explained with the assumption that the droplet does not penetrate the film during the initial phase. The top surface is bare, while the bottom surface is covered with the intact film. The bottom boundary of the droplet consists of two interfaces, one between the isotropic liquid and the smectic film, and the second one between the smectic material and air. The bare droplet surface has a higher tension than the film-covered bottom surface, but the droplet shape is not in equilibrium. The radius of curvature of the upper surface increases continuously, while that of the lower surface decreases.

In most experiments, a rapid decrease of R_b is observed after about 250 μ s. This is already indicated in Figure 4 and is more evident in the images in Figure 5. The two curvatures become comparable, and the droplet sinks into a nearly symmetrical position, with the center of mass near the film level. Obviously, the upper droplet surface is wetted by smectic material during this phase.

Thereafter, the droplet shape flattens within several hundred microseconds. The film tension pulls the droplet material outward at the circular contact line, causing an expansion of the droplet in the film plane. The time scale of this flattening is determined by the smectic film, not by the droplet. Since the Ohnesorge number of the droplet is 0.037, capillary force effects dominate viscosity

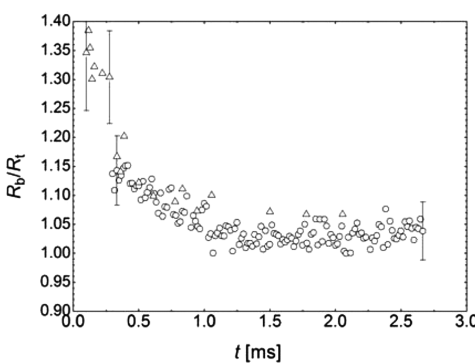
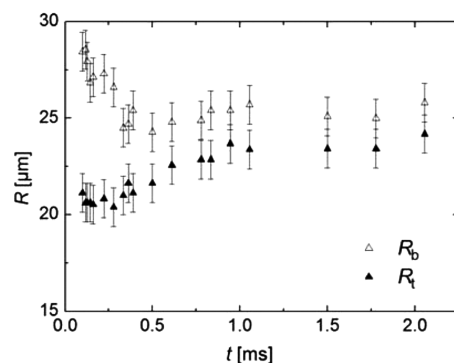


Figure 4. (Left) Change of the radii of curvature over time. R_b and R_t are the radii of bottom and top caps for a droplet with impact velocity 0.4 m/s. (Right) Ratio of the radii. The ratio is mainly influenced by the ratio of interface tensions on the two caps. Triangles are determined manually and circles automatically (see text).

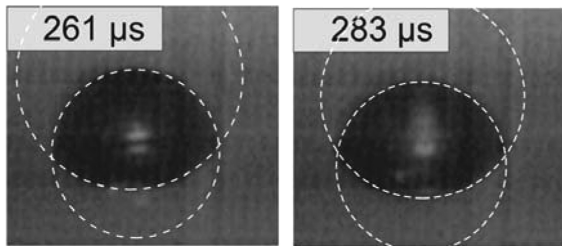


Figure 5. Rapid shape change of a droplet with high impact velocity after 260 μ s. Circular arcs fitted to the upper and lower spherical caps are shown as dashed lines. While the fit to the upper cap is relatively constant, the radius of curvature of the lower cap dramatically decreases, approaching that of the upper cap. We conclude that one of the surfaces changes its structure.

effects. Lamb's model estimates oscillations in the megahertz range. This gives rise to the assumption that a free droplet without the film can change its shape very fast. But the film material around the droplet must reorganize the smectic layers in the film plane, and this sets the limiting conditions. The rapid changes seen in Figure 5 can be explained with the same idea: While the smectic material wets the upper droplet surface, this material is taken from the surrounding film and the droplet flattens rapidly in the plane.

When the two caps of the droplet are completely covered with liquid crystal, both interfaces should attain nearly the same tensions, and the radius ratio should gradually approach 1. In fact, the droplets are not symmetric even after 3 ms; the radius ratio shown in Figure 4 remains systematically larger than 1. We have no conclusive explanation for this systematic deviation, but we give a plausible hypothesis: The film at the bottom of the droplet consists of the smectic mesogens in normal orientation to the interface, as in the surrounding film. At the top, the smectic material that wets the surface is exposed to strong shear flow; this will lead to a certain flow alignment so that the smectic mesogens cover the droplet in planar rather than homeotropic alignment. The two tensions of the smectic material with different orientations respective to the surface, $\sigma_{\text{sm}}^{\parallel}$ and $\sigma_{\text{sm}}^{\perp} (\equiv \sigma_{\text{sm}}^{\perp})$, need not be the same. Unfortunately, there are no literature data available about the anisotropy of the smectic surface tensions. At longer time scales, this difference should vanish.

During the flattening process, we analyze the droplet shapes and extract the contact angles of both caps respective to the film plane. The relevant parameters are defined in Figure 6: on the left-hand side is the sketch of the droplet and definition of the geometrical quantities, while on the right we sketch schematically the enlarged part of the interface between droplet and film.

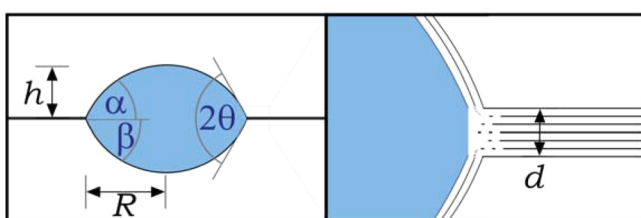


Figure 6. Cross section of a droplet in a smectic film defining the parameters h , R , and d , the inner opening angle 2θ , and the two inner contact angles α and β for the upper and lower cap of the droplet. The contact line contains numerous defects, hence the smectic layer details are not shown there.

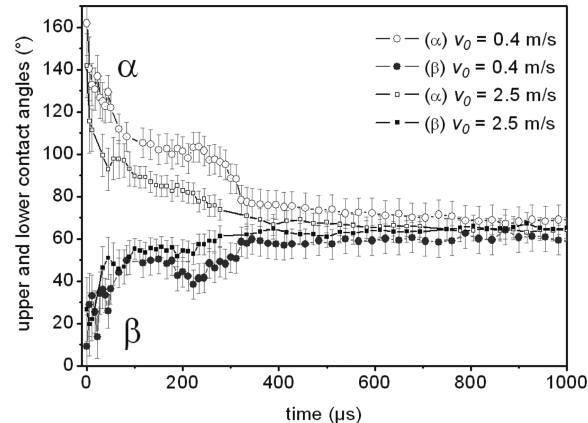


Figure 7. Evolution of contact angles of upper and lower spherical caps at the surrounding film for the fastest and slowest droplets.

Figure 7 shows the evolution of the upper and lower contact angles. (More results for contact angle evolution of droplets with different impact speeds can be found in Supporting Information.) The lower angle starts near 0° when the droplet initially lies on the slightly deflected film. The upper angle starts, depending upon impact velocities, between 160° (slow droplets) and 120° (fast droplets). In this geometry, forces acting on the droplet boundary are not in equilibrium, which requires that

$$\sigma_t \cos \alpha + \sigma_b \cos \beta = 2\sigma_{\text{sm}} \quad (3)$$

In eq 3, σ_t and σ_b denote interface tensions at the top and bottom surfaces of the droplet. For the final droplet shape in equilibrium, if the tensions of its two surfaces were equal, we would have $\sigma_b = \sigma_t = \sigma_{\text{droplet}}$, $\alpha = \beta = \theta$, and

$$\sigma_{\text{droplet}} \cos \theta = \sigma_{\text{sm}}$$

This equation is equivalent to^{46,51}

$$\sigma_{\text{sm}} = \sigma_{\text{droplet}} \frac{R^2 - h^2}{R^2 + h^2} \quad (4)$$

In eq 4, the film thickness d is not considered, because it is at least 1 order of magnitude smaller than the droplet height h . Since σ_{droplet} is higher than the surface tension of the film σ_{sm} , the droplet remains confined and its equilibrium shape consists of two spherical caps. (If the surface tension of the droplet were lower than that of the film, the droplet would flatten continuously to cover the whole film area between the supporting frames.)

On the way to this equilibrium, α and β approach each other continuously (Figure 7), and the time constant of their dynamics is on the order of 200 μ s, practically independent of impact velocities. As noted above, the time scale is set by the retracting freely suspended film. It stretches the droplet, as long as the film tension is larger than the sum of both in-plane components of the forces related to σ_b and σ_t . While the bottom contact angle β performs a rather gradual slow relaxation, the upper contact angle α shows a certain jump after 200–300 μ s (see discussion of the radii of curvature). This is related to the noticeable change in the ratio of curvatures.

An equilibrium angle of $\theta = 66^\circ$ is reached for all droplets after about 1 ms. This angle establishes the equilibrium of droplet and film tensions (eq 4), and it can be used to compare the involved interfaces of film and droplet. The surface tension of the smectic material was estimated from the surface tensions of components of the mixture as $\sigma_{\text{sm}} \approx 22.3$ mN/m. Using this value, one finds an

interface tension of the droplet of $\sigma_{\text{droplet}} = 55 \text{ mN/m}$. This is the average of σ_t and σ_b , which might differ by about 5% from each other. It represents the sum of the smectic-to-air and smectic-to-droplet fluid interface tensions. When the aqueous ethylene glycol 5% solution with a surface tension of 66.38 mN/m is considered,⁵⁸ coverage of the bare ethylene glycol/water mixture with the smectic material apparently reduces the droplet surface tension by about 17%.

A comparison with literature data is not available, since there are very few studies of interface tensions of smectic liquid crystals

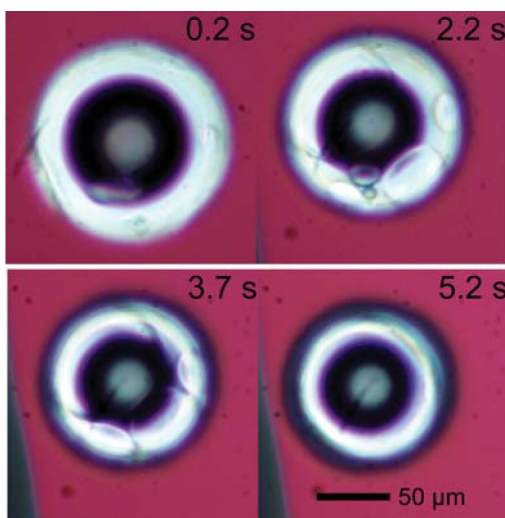


Figure 8. Top views of an ethylene glycol/water mixture droplet, enclosed by a meniscus, in a 500 nm thick smectic film. The elapsed time after impact is given. Already after 0.2 s, the droplet is surrounded by a bright wedge of smectic material. In the subsequent images, one can see excess material climb up the meniscus and successively cover the droplet. After 5.2 s, the top layers have merged in the center, covering the droplet completely. When the first and the last image are compared, it is obvious that the droplet slightly changes its width (it gradually returns to sphere shape).

with respect to water or aqueous solutions. In a previous investigation of smectic films (of a different material than in this study) in a water/surfactant mixture, an interface tension on the order of 6.3 mN/m was reported.⁵⁹ In the absence of surfactants, as in the present case, the interface tension to water is expected to be considerably larger,⁶⁰ but no reliable values exist.

Meniscus Formation. The final images in the sequences of Figure 2 still do not correspond to equilibrium situations. On a longer time scale, the film material continues to reorganize around the droplet and to grow a meniscus. The smectic material starts to cover the sides of the droplet in order to reduce the free surface. After a few seconds, the droplet is enclosed by a meniscus.

Figure 8 was taken with a color camera in reflection microscopy. One can see the formation of a pronounced bright ring around the droplet on a time scale of a few seconds. This is a wedge-shaped flat meniscus (see Figure 9), which in the beginning has roughly twice the radius of the droplet. The uniform purple appearance of the surrounding film indicates that it retains its original uniform thickness, clearly separated from the meniscus, which is typical for menisci of smectic FSF.^{51,53,61}

Figure 9 shows a side view of a droplet after resting 10 min in the film. It is decorated with a meniscus that has grown to approximately 150 μm outer diameter, which gives the complete inclusion a discus-like appearance. In this image, it is impossible to distinguish the aqueous droplet material from the liquid crystal decoration; the whole object appears dark in transmitted light.

In order to distinguish the droplet from its meniscus, a fluorescent dye was added to the droplet material in the dispenser. This allows us to identify the distribution of the water/ethylene glycol mixture in the film plane. The dye remains in the droplet material at least for several seconds.

Figure 10a-c presents a droplet 15 seconds after impact. The bright light microscopy image Figure 10a shows the extension of the meniscus around the droplet. The fluorescent microscopy image Figure 10b of the same droplet visualizes the distribution of the droplet containing the fluorescent dye. Both images are superimposed in Figure 10c. The spot containing the dye has a diameter of 42 μm , approximately the diameter of the spherical

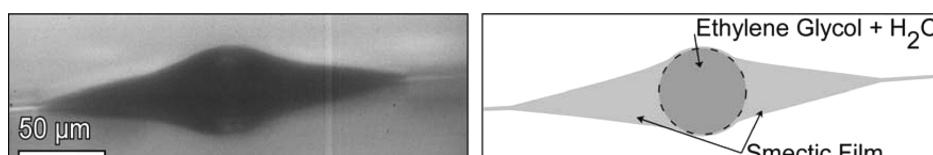


Figure 9. Side view of a droplet 10 min after impact. The image on the left-hand side was taken in transmitted light. The level of the smectic film is seen at the sides as faint bright stripes. The image to the right sketches the assumed cross section.

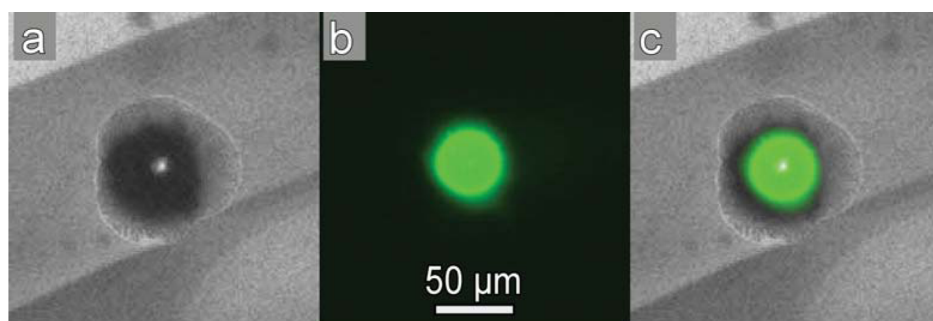


Figure 10. Top views of a droplet 15 s after impact: (a) microscopic image in transmission, (b) fluorescence microscopic image, and (c) superimposed image of both. The microscopic image (a) clearly shows the extension of the complete inclusion with its meniscus. The diagonal edges are layer steps of the smectic film. The circumference of the droplet itself can be found from the fluorescent image (b).

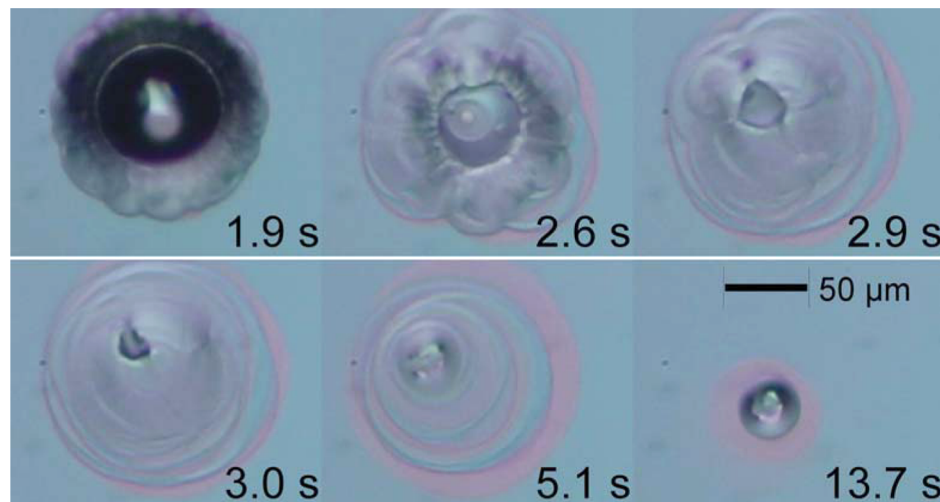


Figure 11. In this figure, a pure water droplet in a smectic FSF and its evaporation is shown. The film thickness is about 1 μm . In each image, the elapsed time after impact is given. The droplet initially hits the film and transforms into a shape formed by two spherical caps, but in this case the smectic material does not wet the free droplet surface. Consequently, the droplet evaporates quickly, and 3 s after the impact only a small portion remains, almost completely immersed in the smectic meniscus. The final image after 13.7 s shows a tiny remnant of the water droplet, now completely enclosed by smectic material.

droplet before impacting the film. Around the droplet, the meniscus extends to a diameter of 96 μm . The outer border of the meniscus is not necessarily circular as evident in Figure 10a, the image may not reflect the final equilibrium shape of the meniscus. We note that the droplet in these images is already embedded almost entirely in smectic material, therefore it returns to spherical shape. The projection of the droplet onto the film plane therefore has a radius that is in good approximation equal to the original droplet size.

Finally, we show that pure water droplets lead to a completely different long-time behavior. Figure 11 shows an example of a droplet consisting of pure distilled water that has been shot onto a smectic film. Here, the upper droplet cap is not wetted completely by the liquid crystal. Consequently, the droplet evaporates rapidly at its free surface. The smectic material that forms a meniscus around the water droplet finally encloses a tiny remnant of the original droplet, retaining only a few percent of the original water content. After 3 s, the height of the wedged smectic material can be estimated from the interference colors to be several micrometers, and the lateral extension of the wedge is about 100 μm . The meniscus material subsequently redistributes again in the film plane. This can be seen in the last image of Figure 11, where the meniscus has shrunk to about one-sixth of its original area and to a height of approximately 200 nm.

CONCLUSIONS

In this study, we investigated the impact of microscopic droplets of a water/ethylene glycol mixture on freely suspended smectic films by use of a microdroplet dispenser that can be precisely positioned near the film. The Ohnesorge number was well below 0.01, and the Weber number varied from 0.1 to 3.8. For the droplet diameters of this study, surface tension dominates the impact behavior. The droplet impact was found to consist of a simple deposition without splashing, followed by a steady immersion in the film and meniscus formation. In addition to dissipation through viscosity of a droplet, the freely suspended film absorbs impact energy. Thus, compared to the work of Son et al.,³⁷ who have studied similar droplet sizes on solid substrates, our droplets show even less deformation.

Initially, the droplet rests on the intact smectic film, even if it hits the film at velocities of 2.5 m/s. The same geometry has been

proposed for the equilibrium description of colloidal silica particles on freely suspended films by Conradi et al.⁶² In contrast to that experiment, where the authors assumed that the upper surface of the beads remained bare during the experiment, our droplets are wetted completely within approximately 1 ms after impact.

After immersion, the droplets develop a lentil-like shape with its two spherical caps sticking out of the film plane. Comparing droplets with different impact velocities, we found that a higher impact velocity slightly accelerates the immersion process without changing it qualitatively. The experimental setup enables a measurement of the contact angle of the immersed droplet, with the possibility to compare interface tensions of droplet and film. When we assume a surface tension of the film of $\sigma_{\text{sm}} = 22.3 \text{ mN/m}$, which is a typical value for smectic materials, we obtain an average tension of 55 mN/m for the droplet to smectic surface layer to air interface.

A meniscus is formed around the droplet within a few seconds after impact. Inside the meniscus, the droplet returns to spherical shape. Menisci shapes around glycerol droplets in smectic C films have been studied in detail earlier.⁵³ The menisci observed here are geometrically very similar, but the smectic A films do not develop corona patterns.

When multiple droplets are shot onto the same position in the film within a few hundred milliseconds, they coalesce and form larger drops. By this method, one can control the sizes of drops in discrete steps and prepare inclusions with more than 100 μm diameter. Furthermore, impact parameters can be varied such that droplets tunnel the free-standing films, whereby they are encapsulated in a thin smectic layer or reflected by the film. These scenarios will be described elsewhere.

Pure water droplets are not suitable for the creation of inclusions in freely suspended films because they evaporate quickly, leaving only irregular and not-well-reproduced remnants in the film.

ASSOCIATED CONTENT

S Supporting Information

One figure showing additional measurements of the evolution of contact angles for droplets with different impact velocities. This material is available free of charge via the Internet at <http://pubs.acs.org>.

AUTHOR INFORMATION

Corresponding Authors

*E-mail sarah.doelle@ovgu.de; fax +49 391 67 18108; tel +49 391 67 20098.

*E-mail ralf.stannarius@ovgu.de; fax +49 391 67 18108; tel +49 391 67 20098.

Present Address

[†]Saarland University, D-66041 Saarbrücken, Germany.

Notes

The authors declare no competing financial interest.

ACKNOWLEDGMENTS

We thank Alexey Eremin for stimulating discussions and Wolfgang Weissflog for the supply of mesogenic material. DFG is acknowledged for support within Project STA 425-28, and the German Space Administration, DLR, for support within Project OASIS-CO.

REFERENCES

- (1) Worthington, A. M. *The Splash of a Drop; The Romance of Science*; Society for Promoting Christian Knowledge: London, 1895.
- (2) Vandewalle, N.; Terwagne, D.; Mullenens, K.; Gilet, T.; Dobolo, S. Dancing Droplets onto Liquid Surfaces. *Phys. Fluids* **2012**, *18*, No. 091106.
- (3) Thoroddsen, S. T.; Thoraval, M.-J.; Takehara, K.; Etoh, T. G. Droplet Splashing by a Slingshot Mechanism. *Phys. Rev. Lett.* **2011**, *106*, No. 034501.
- (4) Thoroddsen, S. T.; Takehara, K.; Etoh, T. G.; Hatsuki, Y. Puncturing a Drop Using Surfactants. *J. Fluid Mech.* **2005**, *530*, 295–304.
- (5) Li, E. Q.; Al-Otaibil, S. A.; Vakarelski, I. U.; Thoroddsen, S. T. Satellite Formation during Bubble Transition through an Interface between Immiscible Liquids. *J. Fluid Mech.* **2014**, *744*, R1.
- (6) Thoroddsen, S. T.; Thoraval, M.-J.; Takehara, K.; Etoh, T. G. Micro-Bubble Morphologies following Drop Impacts onto a Pool Surface. *J. Fluid Mech.* **2012**, *708*, 469–479.
- (7) Thoraval, M.-J.; Takehara, K.; Etoh, T. G.; Popinet, S.; Ray, P.; Josserand, C.; Zaleski, S.; Thoroddsen, S. T. von Karman Vortex Street within an Impacting Drop. *Phys. Rev. Lett.* **2012**, *108*, No. 264506.
- (8) Thoraval, M. J.; Thoroddsen, S. T. Contraction of an Air Disk Caught between Two Different Liquids. *Phys. Rev. E* **2013**, *88*, No. 061001.
- (9) Zhang, L. V.; Toole, J.; Fezzaa, K.; Deegan, R. D. Evolution of the Ejecta Sheet from the Impact of a Drop with a Deep Pool. *J. Fluid Mech.* **2012**, *690*, 5.
- (10) Jiang, T.; Ouyang, J.; Li, X.; Ren, J.; Wang, X. Numerical Study of a Single Drop Impact onto a Liquid Film up to the Consequent Formation of a Crown. *J. Appl. Mech. Tech. Phys.* **2013**, *54*, 720–728.
- (11) Nikolopoulos, N.; Strotos, G.; Nikas, K. S.; Gavaises, M.; Theodorakakos, A.; Marengo, M.; Cossali, G. E. Experimental Investigation of a Single Droplet Impact onto a Sessile Drop. *Atomization Sprays* **2010**, *20*, 909–922.
- (12) Focke, C.; Kuschel, M.; Sommerfeld, M.; Bothe, D. Collision between High and Low Viscosity Droplets: Direct Numerical Simulations and Experiments. *Int. J. Multiphase Flow* **2013**, *56*, 81–92.
- (13) Rioboo, R.; Bauthier, C.; Conti, J.; Vou, M.; de Coninck, J. Experimental Investigation of Splash and Crown Formation during Single Drop Impact on Wetted Surfaces. *Exp. Fluids* **2003**, *35*, 648–652.
- (14) Josserand, C.; Zaleski, S. Droplet Splashing on a Thin Liquid Film. *Phys. Fluids* **2003**, *15*, 1650–1657.
- (15) Pan, K.-L.; Hung, C.-Y. Droplet Impact upon a Wet Surface with Varied Fluid and Surface Properties. *J. Colloid Interface Sci.* **2010**, *352*, 186–193.
- (16) Thoraval, M.-J.; Takehara, K.; Etoh, T. G.; Thoroddsen, S. T. Drop Impact Entrapment of Bubble Rings. *J. Fluid Mech.* **2013**, *724*, 234–258.
- (17) Rioboo, R.; Vou, M.; Adao, H.; Conti, J.; Vaillant, A.; Seveno, D.; de Coninck, J. Drop Impact on Soft Surfaces: Beyond the Static Contact Angles. *Langmuir* **2010**, *26*, 4873–4879.
- (18) Driscoll, M. M.; Nagel, S. R. Ultrafast Interference Imaging of Air in Splashing Dynamics. *Phys. Rev. Lett.* **2011**, *107*, No. 154502.
- (19) de Ruiter, J.; Oh, J. M.; van den Ende, D.; Mugele, F. Dynamics of Collapse of Air Films in Drop Impact. *Phys. Rev. Lett.* **2012**, *108*, No. 074505.
- (20) Kolinski, J. M.; Rubinstein, S. M.; Mandre, S.; Brenner, M. P.; Weitz, D. A.; Mahadevan, L. Skating on a Film of Air: Drops Impacting on a Surface. *Phys. Rev. Lett.* **2012**, *108*, No. 074503.
- (21) Latka, A.; Strandburg-Peshkin, A.; Driscoll, M. M.; Stevens, C. S.; Nagel, S. R. Creation of Prompt and Thin-Sheet Splashing by Varying Surface Roughness or Increasing Air Pressure. *Phys. Rev. Lett.* **2012**, *109*, No. 054501.
- (22) Bischofberger, I.; Mauser, K. W.; Nagel, S. R. Seeing the Invisible-Air Vortices around a Splashing Drop. *Phys. Fluids* **2013**, *25*, No. 091110.
- (23) Lee, J. S.; Weon, B. M.; Je, J. H.; Fezzaa, K. How Does an Air Film Evolve into a Bubble during Drop Impact? *Phys. Rev. Lett.* **2013**, *109*, No. 204501.
- (24) Moore, M. R.; Ockendon, J. R.; Oliver, J. M. Air-Cushioning in Impact Problems. *IMA J. Appl. Math.* **2013**, *78*, 818–838.
- (25) Hicks, P. D.; Purvis, R. Liquid-Solid Impacts with Compressible Gas Cushioning. *J. Fluid Mech.* **2013**, *735*, 120–149.
- (26) Gilet, T.; Bush, J. W. M. Droplets Bouncing on a Wet, Inclined Surface. *Phys. Fluids* **2012**, *24*, No. 122103.
- (27) Koplik, J.; Zhang, R. Nanodrop Impact on Solid Surfaces. *Phys. Fluids* **2013**, *25*, No. 022003.
- (28) Yarin, A. Drop Impact Dynamics: Splashing, Spreading, Receding, Bouncing. *Annu. Rev. Fluid Mech.* **2006**, *38*, 159–192.
- (29) Thoroddsen, S. T.; Etoh, T. G.; Takehara, K. High-Speed Imaging of Drops and Bubbles. *Annu. Rev. Fluid Mech.* **2008**, *40*, 257.
- (30) Rein, M. Phenomena of Liquid Drop Impact on Solid and Liquid Surfaces. *Fluid Dyn. Res.* **1993**, *12*, 61–93.
- (31) Cossali, G. E.; Coghe, A.; Marengo, M. The Impact of a Single Droplet on a Wetted Solid Surface. *Exp. Fluids* **1997**, *22*, 463–472.
- (32) Wang, A.-B.; Chen, C.-C. Splashing Impact of a Single Drop onto Very Thin Liquid Films. *Phys. Fluids* **2000**, *12*, 2155.
- (33) Fell, D.; Sokuler, M.; Lembach, A.; Eibach, T. F.; Liu, C.; Bonaccorso, E.; Auernhammer, G. K.; Butt, H.-J. Drop Impact on Surfactant Films and Solutions. *Colloid Interface Sci.* **2013**, *291*, 1963–1976.
- (34) Schiaffino, S.; Sonin, A. A. Molten Droplet Deposition and Solidification at Low Weber Numbers. *Phys. Fluids* **1997**, *9*, 3172.
- (35) Ukiwe, C.; Mansouri, A.; Kwok, D. Y. The Dynamics of Impacting Water Droplets on Alkanethiol Self-Assembled Monolayers with Co-Adsorbed CH₃ and CO₂H Terminal Groups. *J. Colloid Interface Sci.* **2005**, *285*, 760–768.
- (36) Driscoll, M. M.; Stevens, C. S.; Nagel, S. R. Thin Film Formation during Splashing of Viscous Liquids. *Phys. Rev. E* **2010**, *82*, No. 036302.
- (37) Son, Y.; Kim, C.; Yang, D. H.; Ahn, D. J. Spreading of an Inkjet Droplet on a Solid Surface with a Controlled Contact Angle at Low Weber and Reynolds Numbers. *Langmuir* **2008**, *24*, 2900–2907.
- (38) Gentner, F.; Rioboo, R.; Baland, J. P.; de Coninck, J. Low Inertia Impact Dynamics for Nanodrops. *Langmuir* **2004**, *20*, 4748–4755.
- (39) Gilet, T.; Bush, J. W. M. The Fluid Trampoline: Droplets Bouncing on a Soap Film. *J. Fluid Mech.* **2009**, *625*, 267.
- (40) Courbin, L.; Stone, H. A. Impact, Puncturing, and the Self-Healing of Soap Films. *Phys. Fluids* **2006**, *18*, No. 091105.
- (41) Kim, I.; Wu, X. L. Tunneling of Micron-Sized Droplets through Soap Films. *Phys. Rev. E* **2010**, *82*, No. 026313.
- (42) Do-Quang, M.; Geyl, L.; Stemme, G.; van der Wijngaart, W.; Amberg, G. Fluid Dynamic Behavior of Dispensing Small Droplets through a Thin Liquid Film. *Microfluidics Nanofluidics* **2010**, *9*, 303–311.
- (43) Nguyen, Z. H.; Atkinson, M.; Park, C. S.; MacLennan, J.; Glaser, M.; Clark, N. Crossover between 2D and 3D Fluid Dynamics in the

Diffusion of Islands in Ultrathin Freely Suspended Smectic Films. *Phys. Rev. Lett.* **2010**, *105*, No. 268304.

(44) Eremin, A.; Baumgarten, S.; Harth, K.; Stannarius, R.; Nguyen, Z. H.; Goldfain, A.; Park, C. S.; MacLennan, J. E.; Glaser, M. A.; Clark, N. A. Two-Dimensional Microrheology of Freely Suspended Liquid Crystal Films. *Phys. Rev. E* **2001**, *63*, No. 031702.

(45) Cluzeau, P.; Poulin, P.; Joly, G.; Nguyen, H. Interactions between Colloidal Inclusions in Two-Dimensional Smectic-C* Films. *Phys. Rev. Lett.* **2011**, *107*, No. 268301.

(46) Schüring, H.; Stannarius, R. Isotropic Droplets in Thin Free Standing Smectic Films. *Langmuir* **2002**, *18*, 9735–9743.

(47) Cluzeau, P.; Joly, G.; Nguyen, H. T.; Dolganov, V. K. Two-Dimensional Ordering of Inclusions in Smectic C Phase. *J. Exp. Theor. Phys. Lett.* **2002**, *75*, 482–486.

(48) Völtz, C.; Stannarius, R. Self-Organization of Isotropic Droplets in Smectic-C Free-Standing Films. *Phys. Rev. E* **2004**, *70*, No. 061702.

(49) Stannarius, R.; Völtz, C. Self-Organization of Isotropic Droplets in Smectic-C Free-Standing Films. *Phys. Rev. E* **2005**, *72*, No. 032701.

(50) Dolganov, P. V.; Nguyen, H. T.; Joly, G.; Dolganov, V. K.; Cluzeau, P. Shape of Nematic Droplets in Smectic Membranes. *EPL* **2007**, *78*, 66001.

(51) Bohley, C.; Stannarius, R. Colloidal Inclusions in Smectic Films with Spontaneous Bend. *Soft Matter* **2008**, *4*, 683–702.

(52) Dolganov, P. V.; Nguyen, H. T.; Joly, G.; Dolganov, V. K.; Cluzeau, P. Different Mechanisms of Nucleation and Self-Organization of Droplets in Ferroelectric Smectic Membranes. *Eur. Phys. J. E* **2008**, *25*, 31–37.

(53) Harth, K.; Stannarius, R. Corona Patterns around Inclusions in Freely Suspended Smectic Films. *Eur. Phys. J. E* **2009**, *28*, 265–272.

(54) Amm, H.; Stannarius, R.; Rossberg, A. G. Optical Characterization of Chevron Formation in Nematic Electroconvection. *Phys. D* **1999**, *126*, 171–188.

(55) Shi, J.; Wang, C.; Surendranath, K.; Kang, V.; Gleeson, J. T. Material Characterization for Electroconvection. *Liq. Cryst.* **2002**, *29*, 877–880.

(56) Miyano, K. Surface Tension Measured by Vibrating Membranes: An Application to Smectic A and B Phases. *Phys. Rev. A* **1982**, *26*, 1820.

(57) Lamb, H. *Hydrodynamics*; Cambridge University Press: Cambridge, U.K., 1932.

(58) Tsierkezos, N. G.; Molinou, I. E. Thermodynamic Properties of Water + Ethylene Glycol at 283.15, 293.15, 303.15, and 313.15 K. *J. Chem. Eng. Data* **1998**, *43*, 989–993.

(59) Harth, K.; Stannarius, R. Measurement of the Interface Tension of Smectic Membranes in Water. *Phys. Chem. Chem. Phys.* **2013**, *15*, 7204.

(60) Kim, J.-W.; Kim, H.; Lee, M.; Magda, J. J. Interfacial Tension of a Nematic Liquid Crystal/Water Interface with Homeotropic Surface Alignment. *Langmuir* **2004**, *20*, 8110.

(61) Harth, K.; Stannarius, R.; Schulz, B.; Bahr, C. Atomic Force Microscopy of Menisci of Free-Standing Smectic Films. *Soft Matter* **2011**, *7*, 7103.

(62) Conradi, M.; Ziherl, P.; Šarlah, A.; Mušević, I. Colloids on Free-Standing Smectic Films. *Eur. Phys. J.* **2006**, *20*, 231.